

# Yellow Oleander Extract as Green Sustainable Inhibitor for Aluminum Corrosion in Hydrochloric Acid Solution

Abd El-Aziz S. Fouda<sup>1,\*</sup> , Safaa. H. Etaiw<sup>2</sup>, Eslam S. El-Hussieny<sup>1</sup>

<sup>1</sup> Department of Chemistry, Faculty of Science, El-Mansoura University, Egypt

<sup>2</sup> Chemistry Department, Faculty of Science, Tanta University, Tanta, Egypt

\* Correspondence: [asfouda@mans.edu.eg](mailto:asfouda@mans.edu.eg) (A.S.F.);

Scopus Author ID 56231506400

Received: 17.07.2022; Accepted: 30.08.2022; Published: 19.02.2024

**Abstract:** In this research, the utilization of Yellow Oleander extract (YOE) as a sustainable green corrosion inhibitor for aluminum in 1M HCl was investigated by utilizing “mass loss (ML), electrochemical frequency modulation (EFM), electrochemical impedance spectroscopy (EIS) and potentiodynamic polarization (PP) measurements. The surface examination was analyzed using atomic force microscopy (AFM) and X-ray photoelectron spectroscopy (XPS) analysis”. The impact of temperature on corrosion behavior with varying doses of YOE was investigated using the ML method at temperatures ranging from 25 to 45 °C. Polarization curves reveal that YOE is classified as a mixed-type inhibitor. Inhibition performance improves with increasing YOE concentration and decreases with increasing temperature”. YOE adsorbed on an aluminum surface complies with Langmuir’s isotherm, which is seen as physisorption. The outcomes attained from chemical and electrochemical tests are in good accord.

**Keywords:** Aluminum corrosion; HCl; Yellow Oleander; EIS; EFM; XPS; AFM.

© 2024 by the authors. This article is an open-access article distributed under the terms and conditions of the Creative Commons Attribution (CC BY) license (<https://creativecommons.org/licenses/by/4.0/>).

## 1. Introduction

Aluminum and its amalgams are a crucial construction material owing to their extraordinary, advanced data and the broad variety of mechanical applications, transcendentally in flying, vehicle, and nuclear units. Al alloys are used in a broad assortment of businesses because of their different appealing properties, such as good mechanical properties, lightweight, high conductivity, and corrosion resistance [1]. “Generally, famous acid inhibitors are organic compounds containing N, S, and O atoms with high inhibition efficiencies [2-5]. The compounds of organic heterocyclic have been utilized for the corrosion inhibition of Fe [6-9], Cu [10], Al [11-13], and different metals [14,15] in various corroding media. However, numerous of these compounds have high hindrance performance, and various of them have unwanted side effects, even in greatly small concentrations, because of their poisonousness to humans, harmful environmental effects, and critical cost [16]. Plant extracts are low-cost and environmentally safe, so they are considered eco-friendly corrosion inhibitors. “Recently, several plant extracts have been utilized as powerful corrosion inhibitors for Al alloy in HCl solutions, such as Garlic [17], Black Mulberry [18], Piper Guineans seed [19], and Red onion skin [20]. The inhibition capability of these extracts is ordinarily referred to as the presence of organic species containing tannins, alkaloids, nitrogen bases, carbohydrates, and proteins in their constituents. These compounds commonly include polar functions with N, O, or S atoms

and have conjugated double or triple bonds with aromatic rings in their molecular structures, which are significant adsorption centers. The Yellow Oleander plant is in the Apocynaceae YOE family. The Latin name for YOE is *Cascabela thevetia*. This plant is native to South & Central America. It contains a milky sap that holds a compound called thevetin, which is used as a heart stimulant. However, it is extremely poisonous in its natural form, as are all parts of plants, especially the seeds. The toxins are cardenolides called Thevetin B and Thevetin A (Cerebroside); others include neriifolin, peruvoside, the toxin, and ruvoside. The plant's toxins have been tested in experiments for uses in biological pest control" [21,22]. This study shows the inhibition features of the YOE and investigates the corrosion protection ability by using ML, PP, EIS, and EFM measurements. The surface analysis of the Al metal was analyzed by using AFM and XPS. The temperature effect on the rate of corrosion and thermodynamic parameters were measured and discussed.

## 2. Materials and Methods

### 2.1. Materials and solutions.

Corrosion examinations have been operated on Al specimens with the chemical constituents: 0.30 Si; 0.60 Fe; 0.10 Cu; 1.40 Mn; 0.05 Mg; 0.05 Cr; and the rest is aluminum. The corrosive solution utilized was demonstrated by diluting analytical reagent grade 34% HCl with double distilled water". The stock solution (1000 ppm) of Yellow Oleander was utilized to prepare the desirable concentrations by dilution with doubly distilled water.

### 2.2. Plant extract preparation.

A fine powder was prepared by grinding the dried Yellow Oleander flower. The resulting powder material of around 250 g was dipped in 0.5-liter dichloromethane for 120 hours and, after that, imperiled to recurrent removal with 5 x 50 mL to extract plant materials. After all the amounts of dichloromethane were evaporated, a solid extract was obtained and then prepared to be used as a corrosion inhibitor. Chemical examinations have exhibited that the major chemical compositions of Yellow Oleander are Thevetin B, Cannogenin, Digitoxigenin, and Cannonigenol [22].

### 2.3. ML method.

Pre-weighed aluminum specimens were immersed in one molar "HCl in the lack and existence of various concentrations of YOE varying from 50 to 300 ppm. After diverse immersion, the specimens were taken out, rinsed with doubly distilled water, dehydrated, and weighted precisely" [23]. The inhibition efficiency (IE%) and surface coverage degree,  $\theta$  of YOE, were determined as follows:

$$IE\% = \theta \times 100 = \left[1 - \frac{W}{W^0}\right] \times 100 \quad (1)$$

"where  $W^0$  and  $W$  are the average ML without and with the inhibitor, separately".

### 2.4. Electrochemical tests.

Electrochemical techniques were done utilizing a typical three-electrode thermostatic cell containing 1 cm<sup>2</sup> Aluminum working electrode, "a reference electrode which was saturated calomel electrode (SCE) and platinum sheet as the counter electrode. The working electrode

was polished utilizing emery paper up to 1200 grades. Then, the Al electrode was washed with double distilled water. This arrangement was immersed in 1 M HCl as perfect destructive media. All tests were achieved at 25°C”.

“The PP measurements were conducted by sweeping the potential from -280 to +200 mV SCE with a sweeping rate of 1 mV s<sup>-1</sup> after the working electrode reached a steady state (30 min) and the open circuit potential (OCP) was obtained. EIS measurements were executed within the frequency run (10<sup>5</sup> to 0.1 Hz) with a plentifulness of 5 mV peak-to-peak utilizing AC signals at open circuit potential. The most parameters concluded from the examination of the Nyquist chart are the polarization resistance R<sub>p</sub> and the capacity of double layer C<sub>dl</sub> which is characterized by:

$$C_{dl} = \frac{1}{2\pi f_{max} R_p} \quad (2)$$

where f<sub>max</sub> is the precise frequency at which the imaginary component of the impedance comes to its greatest values. The productivity of the hindrance and the scope of surface (Θ) obtained from the impedance estimations were characterized by the subsequent relation:

$$\% IE = \left(1 - \frac{R_p^0}{R_p}\right) \times 100 \quad (3)$$

“where R<sub>p</sub> and R<sub>p</sub><sup>0</sup> are the polarization resistance within the presence and absence of the inhibitor, respectively”.

EFM measurements were performed utilizing “2 and 5 Hz frequencies. The base frequency was 0.1 Hz, so the wave repeated after 1 s. The intermodulation spectra include the current response harmonic and intermodulation current peaks. The bigger peaks were utilized to evaluate the corrosion current density (i<sub>corr</sub>), the Tafel slopes (β<sub>a</sub> and β<sub>c</sub>), and the causality factors CF2 and CF3. The open circuit potential was permitted to steady for half an hour after this time; the estimations had recently been started. Tests were performed at room temperature 25 ± 1 °C. Estimations were executed employing Gamry Instrument with Gamry framework. Besides, the Echem analyst v.5.03 program was utilized to plot and fit the outcomes data [24].

### 2.5. Surface morphology using AFM and XPS analyses.

Surface morphology of polished aluminum samples prior to and following immersion in 1 M HCl. in the lack and existence of YOE for 24 hrs was executed utilizing Nano Surf Easy scan 2 Flex AFM instruments. In addition, X-ray photoelectron spectroscopy (XPS) measurements were performed using ESCALAB 250Xi, Thermo Scientific, USA.

## 3. Results and Discussion

### 3.1. ML tests.

Aluminum ML was calculated at various time periods (T), in the lack and existence of different YOE concentrations, Fig. 1. “The %IE is influenced by the YOE concentration. The charts for various doses of the YOE are found below the curve of the destructive media. The ascending YOE concentration diminishes mass loss and increases aluminum corrosion inhibition. The ML results show that the YOE is deemed an effective inhibitor for aluminum corrosion in 1M HCl medium. Likewise, the surface coverage (Θ) and inhibition efficiency increase due to the limited productivity because of the slight layer established by the adsorption of YOE” [25]. The data obtained from the ML method were tabulated in Table 1.

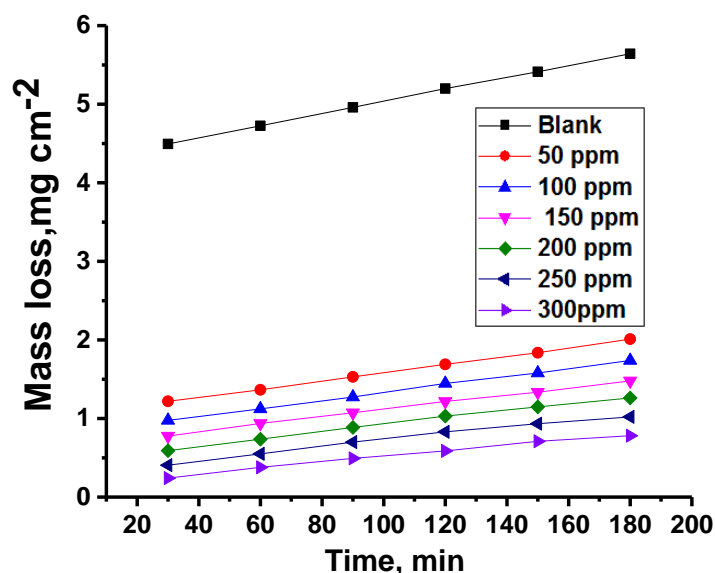


**Figure 1.** Time - ML curves for Al corrosion in one molar HCl in the lack and presence of altered dose of YOE at 25°C.

**Table 1.** Variety of rate of corrosion ( $k_{corr}$ ), coverage of surface ( $\theta$ ), and inhibition efficiency (%IE) with altered doses of YOE after 2 hours of dipping in one molar HCl at various temperatures.

Temp. °C	[Inh]. ppm	Mass loss, mg cm <sup>-2</sup>	$k_{corr}$ , mg cm <sup>-2</sup> min <sup>-1</sup>	$\theta$	%IE
25	<b>Blank</b>	<b>5.20</b>	<b>0.043333</b>	-	-
	50	1.69	0.014075	0.675	67.51
	100	1.45	0.012054	0.722	72.18
	150	1.22	0.010142	0.766	76.59
	200	1.03	0.008588	0.801	80.18
	250	0.83	0.006914	0.840	84.04
	300	0.59	0.004902	0.887	88.69
30	<b>Blank</b>	<b>14.37</b>	<b>0.119743</b>	-	-
	50	6.98	0.058062	0.515	51.51
	100	6.90	0.056040	0.532	53.20
	150	6.57	0.050617	0.577	57.73
	200	6.18	0.045015	0.624	62.41
	250	5.09	0.040126	0.665	66.49
	300	4.86	0.036209	0.698	69.76
35	<b>Blank</b>	<b>20.77</b>	<b>0.173073</b>	-	-
	50	12.24	0.101987	0.411	41.07
	100	11.60	0.096693	0.441	44.13
	150	10.75	0.089544	0.483	48.26
	200	9.72	0.080965	0.532	53.22
	250	8.89	0.074054	0.572	57.21
	300	8.03	0.066923	0.613	61.33
40	<b>Blank</b>	<b>25.31</b>	<b>0.210906</b>	-	-
	50	14.24	0.118654	0.437	43.74
	100	13.60	0.113359	0.463	46.25
	150	12.75	0.106210	0.496	49.64
	200	11.72	0.097632	0.537	53.71
	250	10.89	0.090721	0.570	56.99
	300	10.03	0.083590	0.604	60.37
45	<b>Blank</b>	<b>25.42</b>	<b>0.211823</b>	-	-
	50	14.34	0.119487	0.436	43.59
	100	13.70	0.114193	0.460	46.09
	150	12.85	0.107044	0.495	49.47
	200	11.82	0.098465	0.535	53.52
	250	10.99	0.091554	0.568	56.78
	300	10.13	0.084423	0.601	60.15

### 3.2. PP curves.

Figure 2 demonstrates the polarization curves for aluminum corrosion in one molar HCl corrosive in the lack and existence of diverse YOE doses at room temperature. The protective percent (%IE) and coverage of surface ( $\Theta$ ) are computed from equation (5)

$$\%IE = [(i_{\text{corr}}^{\circ} - i_{\text{corr}}) / i_{\text{corr}}^{\circ}] \times 100 = \theta \times 100 \quad (5)$$

“where  $i_{\text{corr}}^{\circ}$  and  $i_{\text{corr}}$  are the free and inhibited current densities, separately”. Figure 2 shows that both anodic and cathodic lines are moved to lower current densities. In addition, the diminishing of  $i_{\text{corr}}$  is clearly with expanding inhibitor concentration, table 2, demonstrating that the corrosion rate diminishes due to the adsorbed YOE layer and protects the Al surface from HCl corrosion. The highest displacement in  $E_{\text{corr}}$  is  $< 85$  mV, which means that the YOE is a mixed-type inhibitor that influences both anodic and cathodic reactions [26]. Moreover, the Tafel slopes are not changed, meaning that the YOE is adsorbed on a metal surface and hinders the corrosion process by obstructing the active centers without altering the reaction mechanism [27].

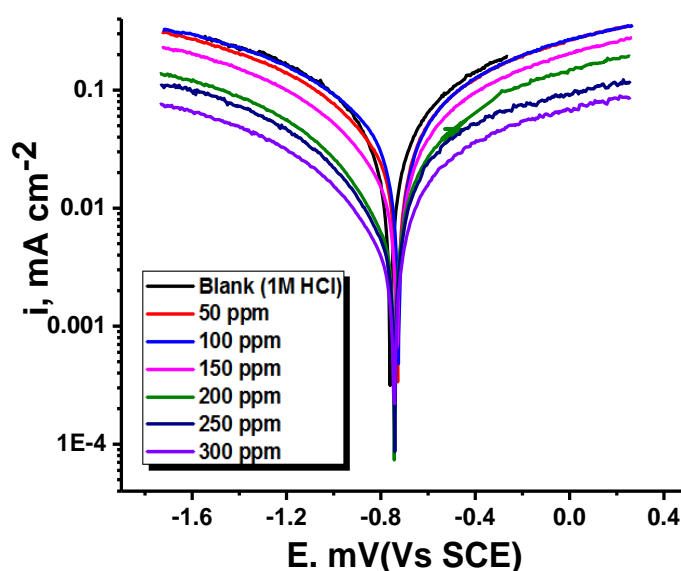


**Figure 2.** PP curves for Al corrosion in one molar HCl solutions in the absence and existence of diverse doses of YOE at room temperature.

**Table 2.** Potential of corrosion ( $E_{\text{corr}}$ ),  $i_{\text{corr}}$ ,  $\beta_c$ ,  $\beta_a$ ,  $\theta$ , and % IE of Al in one molar HCl at room temperature 25°C.

Inhibitor	[Inh] ppm	$-E_{\text{corr}}$ mV vs SCE	$i_{\text{corr}}$ mA cm <sup>-2</sup>	$\beta_a$ mV dec <sup>-1</sup>	$-\beta_c$ mV dec <sup>-1</sup>	CRx10 <sup>3</sup> mpy	$\Theta$	%IE
Blank	0	719	276	251	421	163	---	---
YOE	50	722	137	152	172	59	0.502	50.2
	100	727	127	80	100	57	0.538	53.8
	150	729	82	60	100	37	0.701	70.1
	200	735	61	31	91	11	0.777	77.7
	250	737	55	22	92	5.4	0.799	79.9
	300	739	31	33	93	4.8	0.886	88.6

### 3.3. EIS test.

EIS was achieved to investigate the corrosion inhibition of Al by using YOE after 30 min of dipping. “Figure 3 displays the Nyquist plots for Al in 1 M HCl in the lack and existence of diverse concentrations of YOE. The Nyquist plots revealed that each impedance diagram includes a large capacitive loop at a high-frequency region and a small inductive loop at a low-frequency region. The large capacitive loop is attributed to the relaxation process in the natural

oxide presented on the surface of the Al samples and its dielectric properties, while the small inductive loop is generally attributed to anodic adsorbed intermediates commanding the anodic process [28]. It was shown that the acquired Nyquist curves are not excellent semicircles because of frequency dispersion, and this demeanor can be ascribed to roughness and heterogeneity at the surface of the electrode [24].

Moreover, the diameter of the semi-circular rises with the rising YOE concentration, indicating the adsorption of YOE on the Al surface and creating a protective film. Figure 4 demonstrates the Bode plots for Al in 1 M HCl in the lack and existence of diverse doses of YOE. It was found that as the YOE concentration rises, the total impedance Z increases and the phase angle shifts to more value due to the adsorption of YOE on the Al surface [29].

The circuit equivalent model appears in Figure 5, which was utilized to show the attained impedance information. This demonstration includes “the solution resistance ( $R_s$ ), the charge-transfer resistance of the interfacial corrosion reaction ( $R_{ct}$ ), the inductance (L), the inductive resistance ( $R_L$ ), and the double layer capacitance ( $C_{dl}$ )”. A good fit with this demonstration was achieved by outcomes information. When an inductive circle appears, the resistance of polarization can be computed from the subsequent eq. (6) [30]:

$$R_p = \frac{R_{ct} \times R_L}{R_{ct} + R_L} \quad (6)$$

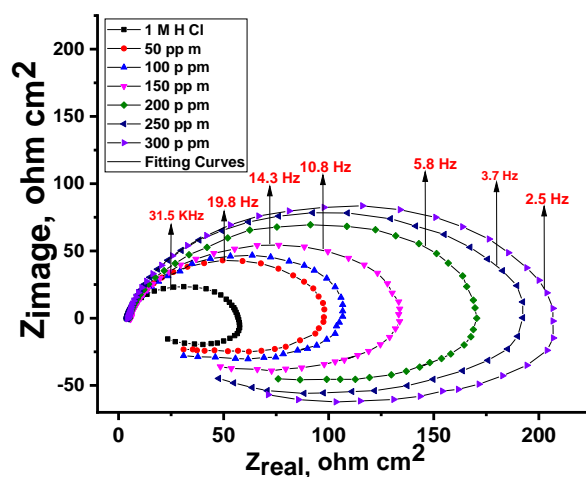


**Figure 3.** Nyquist curves for Al corrosion in 1 M HCl solution in the absence and existence of diverse concentrations of YOE at 25°C.

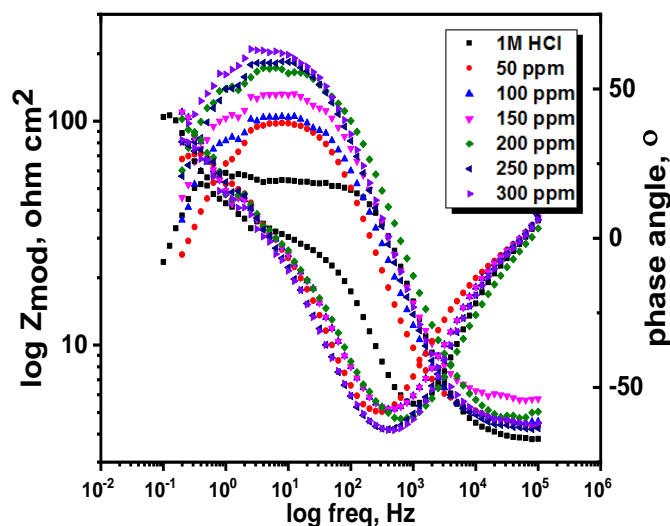


**Figure 4.** Bode curves for Al in the absence and existence of diverse doses of YOE at 25°C.

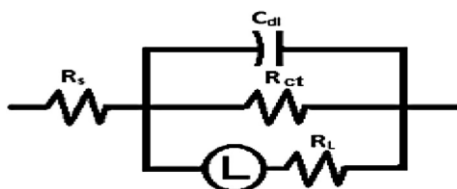


**Figure 5.** Electrical comparable circuit employed to fit the impedance information.

**Table 3.** Parameters acquired from EIS test for Al in 1M HCl in the absence and existence of diverse doses of YOE at 25°C.

Inhibitor	[Inh] ppm	R <sub>ct</sub> Ω cm <sup>2</sup>	C <sub>dl</sub> μFcm <sup>-2</sup>	R <sub>L</sub> Ω cm <sup>2</sup>	R <sub>p</sub> Ω cm <sup>2</sup>	L Ω cm <sup>-2</sup>	Θ	%IE
Blank	0	51.84	177.00	38.12	11.76	13.28	-----	-----
	50	93.27	54.40	71.48	40.47	24.68	0.708	70.8
Yellow Oleander	100	100.53	40.20	76.56	43.46	32.50	0.728	72.8
	150	127.90	31.91	98.02	55.49	40.95	0.787	78.7
	200	169.30	24.28	138.32	76.13	56.89	0.845	84.5
	250	180.60	21.99	148.97	81.63	63.56	0.855	85.5
	300	203.00	20.53	153.32	87.35	73.65	0.864	86.4

EIS data indicate that the R<sub>p</sub> magnitudes increment and the C<sub>dl</sub> magnitudes diminish with the increment of the YOE doses, Table 3. This is often owing to the progressive substitution of H<sub>2</sub>O atoms by the adsorption of the extract atoms on the surface of the metal and diminishing the degree of the disintegration response. The large R<sub>p</sub> magnitudes are for the most part, related to a slower corrosion system [31]. The lessen inside the C<sub>dl</sub> may arise from the lessen of the adjacent dielectric constant and or from the increment of the thickness of the electrical double layer [32], proposing that the inhibitor molecules operate by adsorption at the metal/solution interface. The %IE gotten from EIS tests is near those found from the PP tests.

### 3.4. EFM tests.

EFM is a secure deteriorating technique that recognizes the corrosion current without needing to know the constants of Tafel and by just a little polarization signal. Fig 6 reveals the spectrum of EFM of Al in 1 M HCl solutions by diverse YOE concentrations. From Table 4, adding YOE with diverse doses to the destructive media lessens the corrosion current density, indicating that YOE adsorbed on Al surface formed a protective layer. The causality factors are nearer to hypothetical magnitudes, which, as indicated by the EFM hypothesis [33], ought to demonstrate the validity of the measurements. %IE raises by raising the concentration of YOE, and it tends to be evaluated utilizing equation (5).

**Table 4.** Parameters acquired from EFM technique for Al in 1M HCl in the absence and existence of YOE diverse concentrations.

Inhibitor	[Inh] ppm	i <sub>corr</sub> mA cm <sup>-2</sup>	β <sub>a</sub> mV dec <sup>-1</sup>	β <sub>c</sub> mV dec <sup>-1</sup>	CF-2	CF-3	CRx10 <sup>3</sup> mpy	Θ	%IE
Blank	0	1250	185	196	1.4	2.2	670	---	---
	50	390	30	105	1.9	2.6	240	0.686	68.6
YOE	100	330	29	68	1.2	2.8	210	0.734	73.4
	150	320	27	57	1.8	2.3	202	0.742	74.2
	200	300	24	38	1.7	2.4	150	0.762	76.2
	250	250	18	35	1.3	2.6	146	0.803	80.3
	300	200	15	29	1.9	2.4	132	0.842	84.2

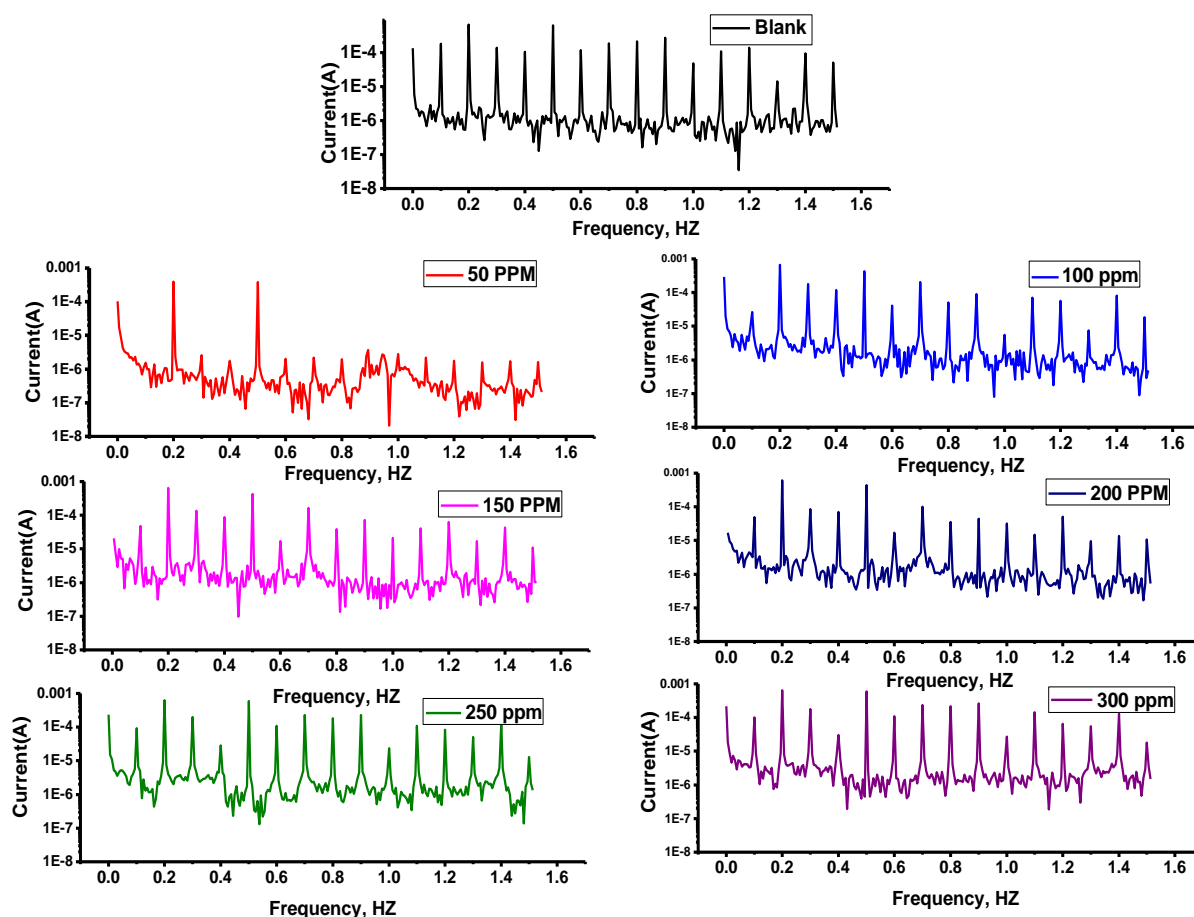


**Figure 6.** Intermodulation spectra for Aluminium corrosion in one molar HCl in the lack and existence of diverse doses of YOE at 25°C.

### 3.5. Adsorption isotherm.

An inhibitor Adsorption on the surface of the metal has been extensively investigated by the use of adsorption isotherms. Organic molecule adsorption takes place due to the contact energy of the inhibitor- surface of the metal, which is greater than that energy of water- surface of metal [34]. For getting the adsorption isotherms, the surface coverage degree ( $\theta$ ) acquired from ML approach was resolved as an inhibitor function concentration (C). The magnitudes of  $\theta$  were then charted to show the most appropriate adsorption model [35]. Many efforts were made to fit the experimental data to several isotherms such as Frumkin, Langmuir, Temkin, Freundlich, isotherms". The outcomes were greatest fitted by Langmuir adsorption isotherm, as found in Fig. 7 [36].

$$\theta / 1 - \theta = K_{ads} C \quad (8)$$

where  $K_{ads}$  is the equilibrium constant of adsorption", which attained from the Langmuir adsorption isotherm slope is correlated to the adsorption free energy  $\Delta G^{\circ}_{ads}$  as follows:

$$K_{ads} = 1/55.5 \exp^{-\Delta G^{\circ}_{ads}/RT} \quad (9)$$

where 55.5 is the molar concentration of water in the solution in  $M^{-1}$ . The values achieved are provided in Table 6.

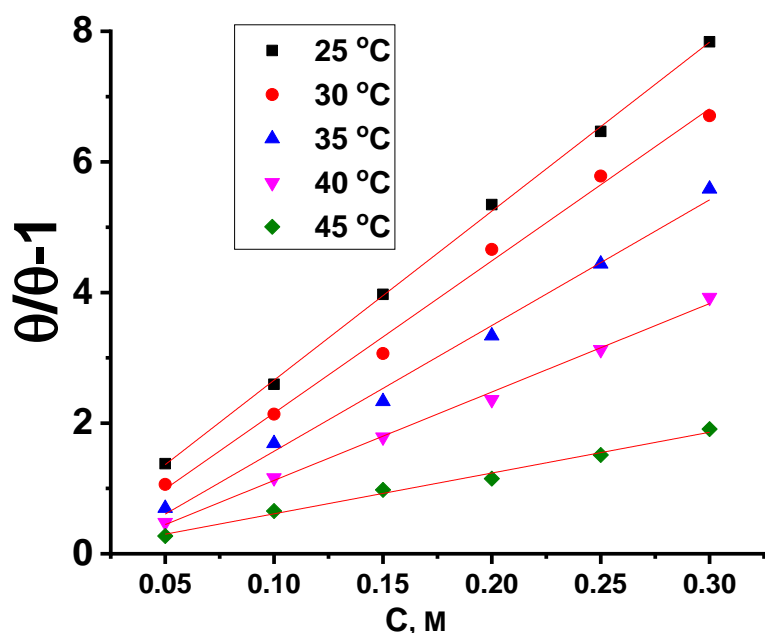


**Figure 7.** Curves of Langmuir adsorption for Al in one molar HCl, including several doses of YOE at different temperatures.

Plot of ( $\Delta G^{\circ}_{ads}$ ) vs Temperature (K) (Fig. 8) provides adsorption heat ( $\Delta H^{\circ}_{ads}$ ) and entropy ( $\Delta S^{\circ}_{ads}$ ) based on the thermodynamic equation (10):

$$\Delta G^{\circ}_{ads} = \Delta H^{\circ}_{ads} - T \Delta S^{\circ}_{ads} \quad (10)$$

Table 5 clearly shows  $\Delta G^{\circ}_{ads}$  magnificent reliance on T, demonstrating the relationship between the obtained thermodynamic data. The negative  $\Delta G^{\circ}_{ads}$  sign data illustrate the spontaneity. For the most part,  $\Delta G^{\circ}_{ads}$  values about  $-20$  kJ/mol or lesser are related to the electrostatic interaction among the charged molecules of YOE and the charged Al surface (physisorption). Still, those around  $-40$  kJ/mol or greater conform to the charge sharing or transfer from YOE molecules to the Al surface to create a coordinated kind of bond (chemisorption). The adsorption was built up to be physical from the given data of  $\Delta G^{\circ}_{ads}$  (from  $-15.47$  to  $-18.02$  kJmol $^{-1}$ ). Endothermic adsorption process ( $\Delta H^{\circ}_{ads} > 0$ ) promotions depend obviously on chemisorption [37]; an exothermic process ( $\Delta H^{\circ}_{ads} < 0$ ) may contain either chemisorption or physisorption or a mixture of both types. The determined  $\Delta H^{\circ}_{ads}$  values present for Yellow Oleander adsorption in an acidic solution demonstrate that this inhibitor may adsorb chemically on the Al surface. The sign of  $\Delta S^{\circ}_{ads}$  in the existence of the YOE is negative, which shows a diminishing in a disorder of the corrosion process on the Al surface [38].

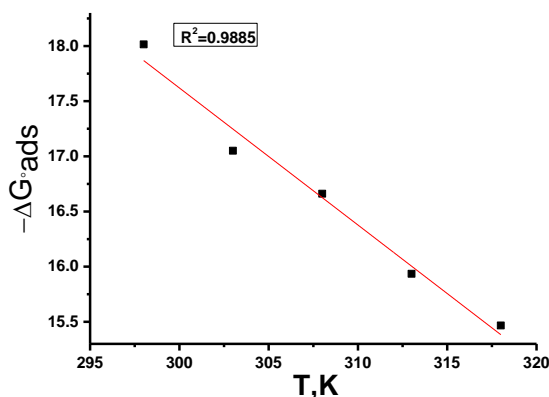


**Figure 8.** The Variety of  $\Delta G^{\circ}_{ads}$  for YOE adsorption on Al surface in 1 M HCl at altered temperatures.

**Table 5.** The adsorption thermodynamic parameters for YOE on Al surface in 1 M HCl at various temperatures.

Inhibitor	Temp. °C	K <sub>ads</sub> × 10 <sup>3</sup> ppm <sup>-1</sup>	-ΔG <sup>o</sup> <sub>ads</sub> kJ mol <sup>-1</sup>	-ΔH <sup>o</sup> <sub>ads</sub> kJ mol <sup>-1</sup>	-ΔS <sup>o</sup> <sub>ads</sub> J mol <sup>-1</sup> K <sup>-1</sup>
Yellow Oleander Extract	25	25	18.0	54.8	123.7
	30	23	17.1		124.8
	35	19	16.6		124.1
	40	13	15.9		124.4
	45	6	15.4		123.9

3.6. The corrosion thermodynamic parameters.

At various temperatures (25-45°C), ML method was accomplished in the existence of diverse concentrations of YOE. It has been discovered that the corrosion rate is directly comparable to the temperature (table 1), which makes %IE diminish with temperature. The corrosion parameter with and without YOE in the temperature variety 25°C-45°C has been summarized in Table 1. E<sub>a</sub>\* for dissolution of Al alloy in 1.0 M HCl was measured by utilizing the Arrhenius equation from the slope of plots as follows:

$$\log k = \frac{-E_a^*}{2.303 RT} + \log A \quad (11)$$

where the corrosion rate is expressed by k, and A is the Arrhenius pre-exponential factor.

The values of “E<sub>a</sub>\* computed from the plotting of log k<sub>corr</sub> versus temperature are demonstrated in Figure 9. The values of E<sub>a</sub>\* for Al in 1M HCl ascend with increasing YOE concentration. Hence, we can induce that the attendance of the YOE generates an energy barrier for corrosion reaction, and this barrier rises with the rising extract concentration. Thus, the protection performance of the extract diminishes noticeably with rising temperature. This result designates that the adsorption of YOE molecules on the Al alloy surface is physisorption” [39]. The entropy change (ΔS\*) and the enthalpy change (ΔH\*) can be computed as follows:

$$k = \left(\frac{RT}{Nh}\right) \exp\left(\frac{\Delta S^*}{R}\right) \exp\left(\frac{\Delta H^*}{RT}\right) \quad (12)$$

where k is the rate of corrosion, h is Planck’s constant, N is Avogadro number, ΔS\* is the entropy of activation, and ΔH\* is the enthalpy of activation. log (k/T) vs 1/T plot (Fig 10) ought to provide a straight line; by using a slope of (ΔH\*/2.303R) and an intercept of [log (R/Nh) + ΔS\*/2.303R], one can calculate magnitudes of ΔS\* and ΔH\* (Tab 6). ΔS\* magnitudes are negative, indicating that the activated complex in the rate-determining step shows association rather than dissociation step [40]. The sign of ΔH\* is (+ve) shows that the adsorption is an endothermic process. Usually, an endothermic process signifies the chemisorption process.

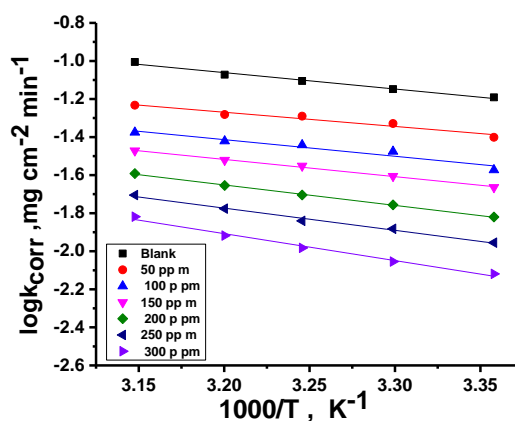


**Figure 9.** Arrhenius curves for Al (k<sub>corr</sub>) after 120 minutes of dipping in 1 M HCl with and without different concentrations of Yellow Oleander extract.

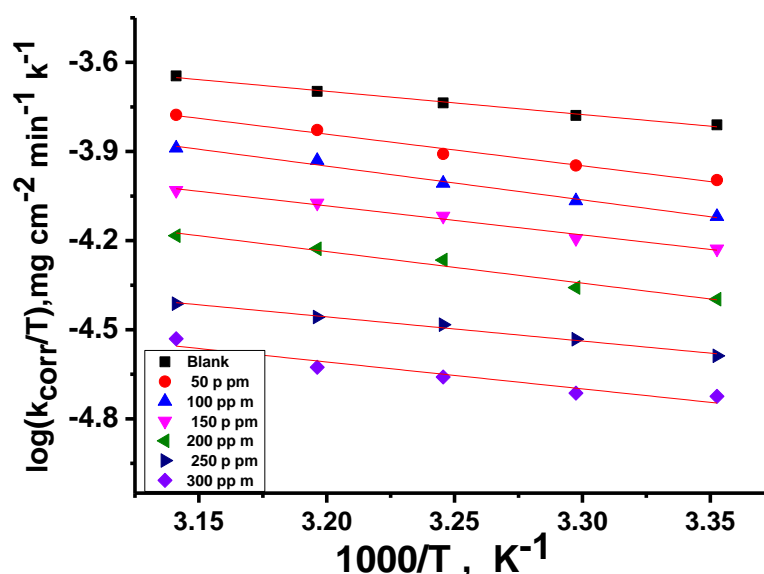


**Figure 10.** Transition-state for Al corrosion in 1 M HCl with and without diverse concentrations of Yellow Oleander extract.

**Table 6.** The thermodynamic activation parameters for Al corrosion in the absence and existence of diverse doses of YOE in one molar HCl.

Conc. ppm	Ea*, kJ mol <sup>-1</sup>	ΔH*, kJ mol <sup>-1</sup>	-ΔS*, J mol <sup>-1</sup> K <sup>-1</sup>
Blank	14.3	11.5	203.5
50	16.7	14.4	205.9
100	17.3	14.8	213.4
150	18.7	16.0	215.7
200	20.6	18.3	220.3
250	22.3	19.6	230.2
300	27.1	24.7	232.9

### 3.7. AFM analysis.

AFM is a significant examination for determining the metal surface roughness at the highest resolution in nanometer fraction [41]. This technique can give insights regarding the shape of the surface of Al, which is helpful for corrosion science research. AFM photos with three dimensional are presented in Figure 11. The average roughness ( $R_a$ ) is shown in Table 7. A proportional view of the relative perspective in Table 7 reveals that the surface of the metal before dipping in HCl acid is smoothed (46.4 nm); after dipping in 1 M HCl, the surface is destroyed, and the roughness rises (760.0 nm) while the Al sample treated with 300 ppm YOE the surface becomes smoother. The roughness reduced (409.1 nm) compared with a blank sample as a sign of the YOE adsorbed on the surface of Al metal creating the protective film.

**Table 7.** AFM roughness data of Yellow Oleander at 300 ppm for 24 hours at 25°C.

Specimen	Average roughness ( $R_a$ ) nm
Al surface (free)	46.4
Al in 1M HCl (blank)	760.0
Al in 1M HCl + 300ppm YOE	409.1

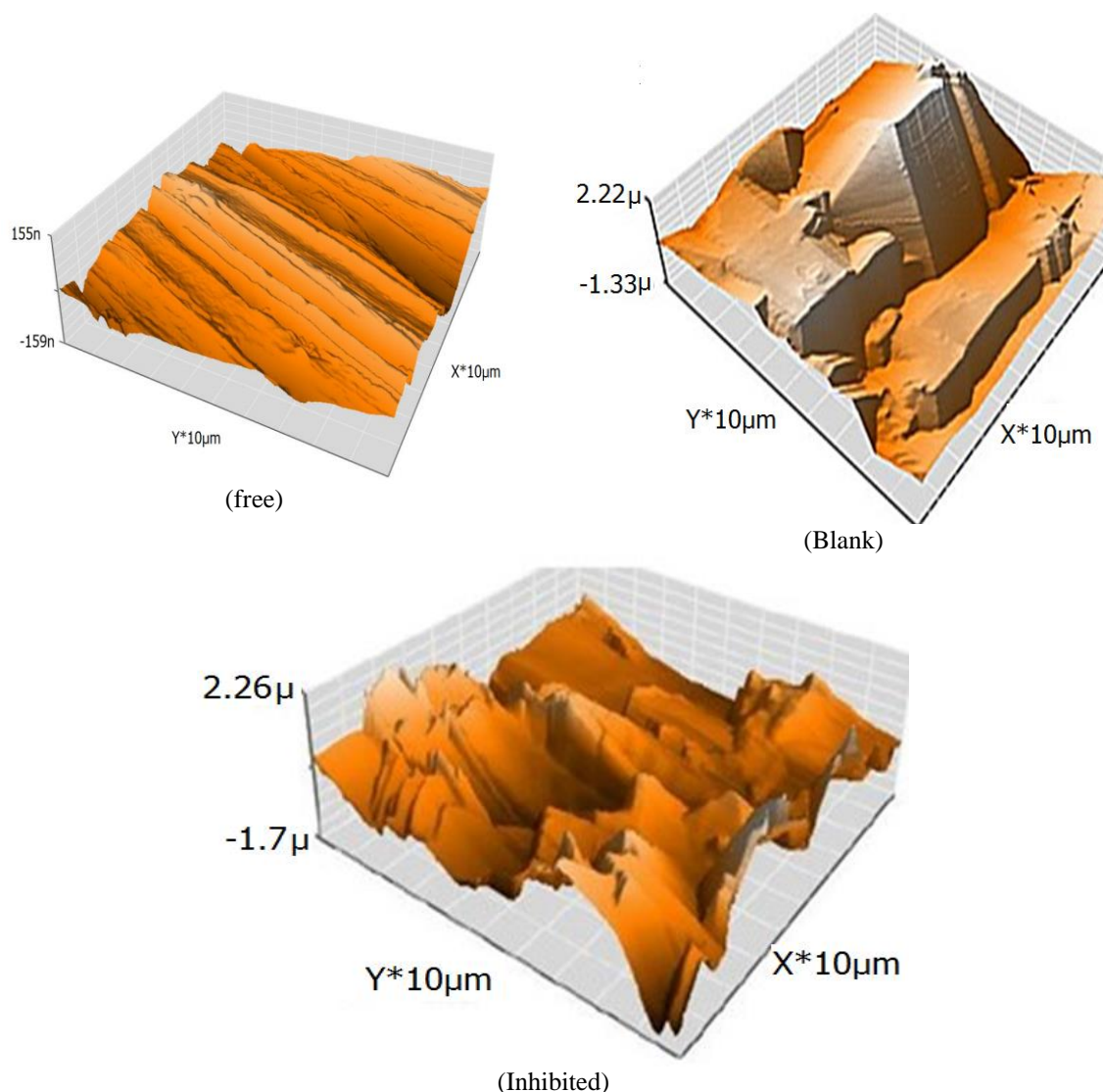


**Figure 11.** 3D AFM images Al metal before dipping in 1 M HCl (free) and after dipping in 1 M HCl (blank) and in the presence of 300 ppm of YOE (inhibited) for 24 hours at 25°C.

### 3.8. XPS technique.

XPS analysis gets reflective knowledge of the chemical nature of the interface between the YOE and the surface of Al. “The spectra are displayed for aluminum surface subsequently soaking in 1 M HCl solution containing 300 ppm of YOE for 24 hours. The XPS deconvoluted profiles of Al 2p, O 1s, Cl 2p, and C 1s appear in Fig. 12. The Al 2p spectrum demonstrated at binding energy (BE) of 74.47 eV (Fig.12a) may be ascribed for Aluminum oxide ( $\text{Al}_2\text{O}_3$ ) [42]. The spectrum of O 1s (Fig.12b) exhibits three peaks, at 530.86 and 531.99 eV, which appointed to Al-O-Al bond (oxide) in  $\text{Al}_2\text{O}_3$  and at 532.98 eV binding energy associated with Al-OH bond (hydroxide) in  $\text{Al}(\text{OH})_3$ . The spectrum of Cl 2p includes 2 peaks situated at 197.81 eV for Cl 2p<sub>3/2</sub> and 199.46 eV for Cl 2p<sub>1/2</sub> (Fig. 12 c). The C1s spectra represent three peaks found at 284.40, 285.93, and 288.90 eV (Fig. 12d). The greatest peak at 284.40 can be ascribed to the C-C, C-H, C=C bond of aromatic rings. Additionally, the peaks placed at 285.93 eV are ascribed to the C-O-C and C-O bonds individually [43]. The peak found at 288.90 eV, which is attributed to O-C=O, C = O, appears that the molecules of YOE have been arranged and adsorbed on the surface of Al”. Lastly, the XPS spectra demonstrated that the protective film created on the surface involves a mix of components, including Carbon and Oxygen atoms, that demonstrate establishing an inhibitive layer of the YOE.

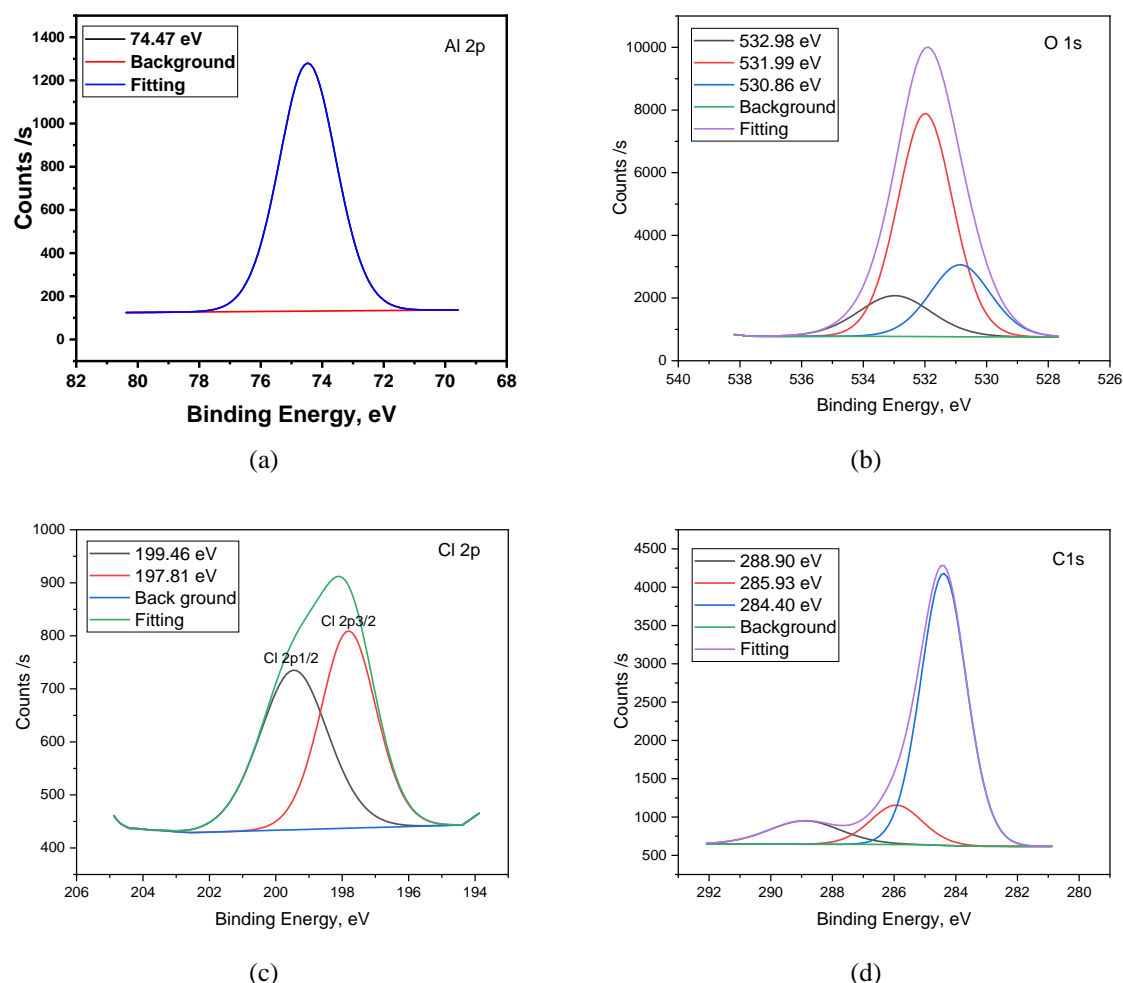


**Figure 12.** XPS deconvoluted profiles of (a) Al 2p, (b) Oxygen 1s, (c) Chlorine 2p, and (d) Carbon 1s, for Al in one molar HCl containing 300 pm YOE.

### 3.9. Mechanism of corrosion inhibition.

Following chemical and electrochemical measurements, the addition of YOE prompts impeding the aluminum corrosion. From the outcomes, the inhibition mechanism involves hindering surface-active sites that adsorbed the YOE. YOE adsorption mechanism includes physisorption according to the values of  $\Delta G^{\circ}_{\text{ads}}$  around  $14 \text{ kJ mol}^{-1}$ . This occurs via the electrostatic attraction between the negative charge on the Al surface and the positive charge of the protonated component in YOE. The inhibitory abilities of these constituents may be attributed to their adsorption using the C=O, OH, etc. groups, in addition to the existence of  $\pi$ -electrons in benzene rings. These organic molecules acquire adsorption at Al's surface, creating an insurance layer that protects the Al surface [44,45].

## 4. Conclusions

Yellow Oleander extract has corrosion-inhibiting action on aluminum in 1 M HCl, as affirmed by chemical, electrochemical, and surface analysis. PP results demonstrated that the YOE hindered both anodic and cathodic reactions (i.e., mixed type inhibitor). %IE of YOE diminished with temperature ascending. The adsorption of YOE complies with the Langmuir isotherm and is considered physisorption. AFM and XPS analyses give information about morphology, the roughness of the Al surface, and the chemical nature between YOE and Al

surface; hence, they confirm the adsorption of YOE on the Al surface. There is a good accord between chemical and electrochemical measurements.

## Funding

This research received no external funding.

## Acknowledgments

All our gratitude to the anonymous referees for their careful reading of the manuscript and valuable comments helped shape this paper to the present form. We thank all laboratory staff of corrosion chemistry from the University of Mansoura (Egypt) for their kind cooperation.

## Conflicts of Interest

The authors declare no conflict of interest.

## References

1. TrabANELLI, G. 1991 Whitney Award Lecture: Inhibitors—An Old Remedy for a New Challenge. *Corrosion* **1991**, *47*, 410-419, <https://doi.org/10.5006/1.3585271>.
2. Singh, D.D.N.; Dey, A.K. Synergistic Effects of Inorganic and Organic Cations on Inhibitive Performance of Propargyl Alcohol on Steel Dissolution in Boiling Hydrochloric Acid Solution. *Corrosion* **1993**, *49*, 594-600, <https://doi.org/10.5006/1.3316090>.
3. Banerjee, G.; Malhotra, S.N. Contribution to Adsorption of Aromatic Amines on Mild Steel Surface from HCl Solutions by Impedance, UV, and Raman Spectroscopy. *Corrosion* **1992**, *48*, 10-15, <https://doi.org/10.5006/1.3315912>.
4. Arab, S.T.; Noor, E.A. Inhibition of Acid Corrosion of Steel by Some S-Alkylisothiuronium Iodides. *Corrosion* **1993**, *49*, 122-129, <https://doi.org/10.5006/1.3299206>.
5. Raspini, I.A. Influence of Sodium Salts of Organic Acids as Additives on Localized Corrosion of Aluminum and Its Alloys. *Corrosion* **1993**, *49*, 821-828, <https://doi.org/10.5006/1.3316005>.
6. Khadraoui, A.; Khelifa, A.; Touafri, L.; Hamitouche, H.; Mehdaoui, R. Acid extract of *Mentha pulegium* as a potential inhibitor for corrosion of 2024 aluminum alloy in 1 M HCL solution. *J. Mater. Environ. Sci.* **2013**, *04*, 663-670.
7. Luo, H.; Guan, Y.C.; Han, K.N. Inhibition of Mild Steel Corrosion by Sodium Dodecyl Benzene Sulfonate and Sodium Oleate in Acidic Solutions. *Corrosion* **1998**, *54*, 619-627, <https://doi.org/10.5006/1.3287638>.
8. Migahed, M.A.; Azzam, E.M.S.; Al-Sabagh, A.M. Corrosion inhibition of mild steel in 1 M sulfuric acid solution using anionic surfactant. *Materials Chemistry and Physics* **2004**, *85*, 273-279, <https://doi.org/10.1016/j.matchemphys.2003.12.027>.
9. Khaled, M.A.; Ismail, M.A.; El-Hossiany, A.A.; Fouda, A.E.-A.S. Novel pyrimidine-bichalcophene derivatives as corrosion inhibitors for copper in 1 M nitric acid solution. *RSC Advances* **2021**, *11*, 25314-25333, <https://doi.org/10.1039/D1RA03603C>.
10. Kumar, S.H.; Karthikeyan, S. Inhibition of mild steel corrosion in hydrochloric acid solution by cloxacillin drug. *J. Mater. Environ. Sci.* **2012**, *3*, 925-934.
11. Al-Sawaad, H.Z.; Al-Mubarak, A.S.; Haddad, A.M. The inhibition effects of dimethylol-5-methyl hydantoin and its derivatives on carbon steel alloy. *J. Mater. Environ. Sci.* **2010**, *1*, 227-238.
12. Fouda, A.S.; El-Mekabaty, A.; Shaaban, I.E.I.; El-Hossiany, A. Synthesis and Biological Evaluation of Novel Thiophene Derivatives as Green Inhibitors for Aluminum Corrosion in Acidic Media. *Protection of Metals and Physical Chemistry of Surfaces* **2021**, *57*, 1060-1075, <https://doi.org/10.1134/S2070205121050075>.
13. Al-Abdali, F.H.; Abdallah, M.; El-Sayed, R. Corrosion inhibition of aluminum using nonionic surfactant compounds with a six membered heterocyclic ring in 1.0 M HCl solution. *Int. J. Electrochem. Sci.* **2019**, *14*, 3509-3523, <https://doi.org/10.20964/2019.04.59>.
14. Bashir, S.; Sharma, V.; Singh, G.; Lgaz, H.; Salghi, R.; Singh, A.; Kumar, A. Electrochemical Behavior and Computational Analysis of Phenylephrine for Corrosion Inhibition of Aluminum in Acidic Medium. *Metallurgical and Materials Transactions A* **2019**, *50*, 468-479, <https://doi.org/10.1007/s11661-018-4957-9>.
15. Satyabama, P.; Rajendran, S.; Nguyen, T.A. Corrosion inhibition of aluminum by oxalate self-assembling monolayer. *Anti-Corrosion Methods and Materials* **2019**, *66*, 768-773, <https://doi.org/10.1108/ACMM-01-2019-2061>.

16. Algaber, A.S.; El-Nemma, E.M.; Saleh, M.M. Effect of octylphenol polyethylene oxide on the corrosion inhibition of steel in 0.5M H<sub>2</sub>SO<sub>4</sub>. *Materials Chemistry and Physics* **2004**, *86*, 26-32, <https://doi.org/10.1016/j.matchemphys.2004.01.040>.
17. Ali, A.I.; Foad, N. Inhibition of aluminum corrosion in hydrochloric acid solution using black mulberry extract. *Journal of Materials and Environmental Science* **2012**, *3*, 917-924.
18. Nwosu, O.; Osarolube, E.; Nnanna, L.A.; Akoma, C.S.; Chigbu, T. Acidic corrosion inhibition of piper guineense seed extract on Al alloy. *American journal of Materials science* **2014**, *4*, 178-183.
19. Ozoemena, C.P.; Charles, M. Computational modeling and statistical analysis on the corrosion inhibition of aluminium in nitric acid solution by ethanolic extract of citrus sinesis seed. *Global Journal of Pure and Applied Chemistry Research* **2019**, *7*, 25-46.
20. Fouda, A.S.; Abdel Azeem, M.; Mohamed, S.A., El-Hossiany, A.; El-Desouky, E. Corrosion Inhibition and Adsorption Behavior of Nerium Oleander Extract on Carbon Steel in Hydrochloric Acid Solution. *Int. J. Electrochem. Sci.* **2019**, *14*, 3932–3948, <https://doi.org/10.20964/2019.04.44>.
21. Singh, K.; Agrawal, K.K.; Mishra, V.; Uddin, S.M.; Shukla, A. A Review on Thevetia peruviana. *International Research Journal of Pharmacy* **2012**, *3*, 74-77.
22. Manh, T.D.; Huynh, T.L.; Thi, B. V.; Lee, S.; Yi, J.; Nguyen Dang, N. Corrosion Inhibition of Mild Steel in Hydrochloric Acid Environments Containing Sonneratia caseolaris Leaf Extract. *ACS omega* **2022**, *7*, 8874-86, <https://doi.org/10.1021/acsomega.1c07237>.
23. Fouda, A.S.; Abdel-Latif, E.; Helal, H.M.; El-Hossiany, A. Synthesis and Characterization of Some Novel Thiazole Derivatives and Their Applications as Corrosion Inhibitors for Zinc in 1 M Hydrochloric Acid Solution. *Russian Journal of Electrochemistry* **2021**, *57*, 159-171, <https://doi.org/10.1134/S1023193521020105>.
24. Fouda, A.S.; El-Ghaffar, M.A.A.; Sherif, M.H.; El-Habab, A.T.; El-Hossiany, A. Novel Anionic 4-Tert-Octyl Phenol Ethoxylate Phosphate Surfactant as Corrosion Inhibitor for C-steel in Acidic Media. *Protection of Metals and Physical Chemistry of Surfaces* **2020**, *56*, 189-201, <https://doi.org/10.1134/S2070205120010086>.
25. Prifiharni, S.; Mashanafie, G.; Priyotomo, G.; Royani, A.; Ridhova, A.; Elya, B.; Soedarsono, J.W. Extract sarampa wood (*Xylocarpus Moluccensis*) as an eco-friendly corrosion inhibitor for mild steel in HCl 1M. *Journal of the Indian Chemical Society* **2022**, *99*, <https://doi.org/10.1016/j.jics.2022.100520>.
26. Kumar, H.; Yadav, V.; Kumari, A. Adsorption, corrosion inhibition mechanism, and computational studies of *Azadirachta indica* extract for protecting mild steel: Sustainable and green approach. *Journal of Physics and Chemistry of Solids* **2022**, *165*, <https://doi.org/10.1016/j.jpcs.2022.110690>.
27. Fouda, A.S.; Motaal, S.M.A.; Ahmed, A.S.; Sallam, H.B.; Ezzat, A.; El-Hossiany, A. Corrosion Protection of Carbon Steel in 2M HCl Using Aizoon canariense Extract. *Biointerface research in applied chemistry* **2021**, *12*, 230–243, <https://doi.org/10.33263/BRIAC121.230243>.
28. Zaher, A.; Aslam, R.; Lee, H. S.; Khafouri, A.; Boufellous, M.; Alrashdi, A. A.; Lgaz, H.; Ouhssine, M. A combined computational & electrochemical exploration of the *Ammi visnaga* L. extract as a green corrosion inhibitor for carbon steel in HCl solution. *Arabian Journal of Chemistry* **2022**, *15*, <https://doi.org/10.1016/j.arabjc.2021.103573>.
29. Fouda, A.S.; Ahmed, R.E.; El-Hossiany, A. Chemical, Electrochemical and Quantum Chemical Studies for Famotidine Drug as a Safe Corrosion Inhibitor for  $\alpha$ -Brass in HCl Solution. *Protection of Metals and Physical Chemistry of Surfaces* **2021**, *57*, 398-411, <https://doi.org/10.1134/S207020512101010X>.
30. Fouda, A.S.; Al-Hazmi, N.E.; El-Zehry, H.H.; El-Hossainy, A. Electrochemical and surface characterization of chondria macrocarpa extract (CME) as save corrosion inhibitor for aluminum in 1M HCl medium. *J Appl Chem.* **2020**, *9*, 362-381.
31. Elgyar, O.A.; Ouf, A.M.; El-Hossiany, A.; Foud, A.S. The Inhibition Action of *Viscum Album* Extract on the Corrosion of Carbon Steel in Hydrochloric Acid Solution. *Biointerface research in applied chemistry* **2021**, *11*, 14344–14358, <https://doi.org/10.33263/BRIAC116.1434414358>.
32. Feng, L.; Zhang, S.; Hao, L.; Du, H.; Pan, R.; Huang, G.; Liu, H. Cucumber (*Cucumis sativus* L.) Leaf Extract as a Green Corrosion Inhibitor for Carbon Steel in Acidic Solution: Electrochemical, Functional and Molecular Analysis. *Molecules* **2022**, *27*, <https://doi.org/10.3390/molecules27123826>.
33. Kouache, A.; Khelifa, A.; Boutoumi, H.; Moulay, S.; Feghoul, A.; Idir, B.; Aoudj, S. Experimental and theoretical studies of *Inula viscosa* extract as a novel eco-friendly corrosion inhibitor for carbon steel in 1 M HCl. *Journal of Adhesion Science and Technology* **2022**, *36*, 988-1016, <https://doi.org/10.1080/01694243.2021.1956215>.
34. Fouda, A.S.; Abd El-Maksoud, S.A.; El-Hossiany, A.; Ibrahim, A. Corrosion Protection of Stainless Steel 201 in Acidic Media using Novel Hydrazine Derivatives as Corrosion Inhibitors. *Int. J. Electrochem. Sci.* **2019**, *14*, 2187-2207, <https://doi.org/10.20964/2019.03.15>.
35. Batah, A.; Chaouiki, A.; El Mouden, O.I.; Belkhaouda, M. H.; Bammou, L.; Salghi, R. Almond waste extract as an efficient organic compound for corrosion inhibition of carbon steel (C38) in HCl solution. *Sustainable Chemistry and Pharmacy* **2022**, *27*, <https://doi.org/10.1016/j.scp.2022.100677>.
36. Motawea, M. M.; El-Hossiany, A.; Fouda, A.S. Corrosion Control of Copper in Nitric Acid Solution using *Chenopodium* Extract. *Int. J. Electrochem. Sci.* **2019**, *14*, 1372–1387, <https://doi.org/10.20964/2019.02.29>.

37. Boukhedena, W.; Deghboudj, S.; Benahmed, M.; Laouer H. Experimental Study and Modeling of the Corrosion Inhibition of Mild Steel in 1M HCl with Novel Friendly Butanolic Extract of Ephedra Major. *Journal of the Mexican Chemical Society* **2022**, *66*, <https://doi.org/10.29356/jmcs.v66i2.1630>.
38. Fouda, A.S.; El-Dossoki, F.I.; El-Hossiany, A.; Sello, E.A. Adsorption and Anticorrosion Behavior of Expired Meloxicam on Mild Steel in Hydrochloric Acid Solution. *Surface Engineering and Applied Electrochemistry* **2020**, *56*, 491–500, <https://doi.org/10.3103/S1068375520040055>.
39. Abdelaziz, S.; Benamira, M.; Messaadia, L.; Boughoues, Y.; Lahmar, H.; Boudjerda, A. Green corrosion inhibition of mild steel in HCl medium using leaves extract of *Arbutus unedo* L. plant: An experimental and computational approach. *Colloids and Surfaces A: Physicochemical and Engineering Aspects* **2021**, *619*, <https://doi.org/10.1016/j.colsurfa.2021.126496>.
40. Vuong, B.X.; Huynh, T.L.; Tran, T.Q.; Vattikuti, S.P.; Manh, T.D.; Nguyen-Tri, P.; Nguyen, A.T.; Van Hien, P.; Dang, N.N. Corrosion inhibition of carbon steel in hydrochloric acid solution by self-formation of a *Malpighia glabra* leaf extract-based organic film. *Materials Today Communications* **2022**, *31*, <https://doi.org/10.1016/j.mtcomm.2022.103641>.
41. Wang, Q.; Zhang, Q.; Liu, L.; Zheng, H.; Wu, X.; Li, Z.; Gao, P.; Sun, Y.; Yan, Z.; Li, X. Experimental, DFT and MD evaluation of *Nandina domestica* Thunb. extract as green inhibitor for carbon steel corrosion in acidic medium. *Journal of Molecular Structure* **2022**, *24*, <https://doi.org/10.1016/j.molstruc.2022.133367>.
42. Fouda, A.S.; El-Gharkawy, E.S.; Ramadan, H.; El-Hossiany, A. Corrosion resistance of mild steel in hydrochloric acid solutions by *Clinopodium acinos* as a green inhibitor. *Biointerface Res Appl Chem.* **2021**, *11*, 9786-9803, <https://doi.org/10.33263/BRIAC112.97869803>.
43. Mahmoud, A.A.; Abdelfattah, M.O.; El-Hossiany, A.; Foud, A.S. Eco-Friendly Approach to Corrosion Inhibition of Copper in HNO<sub>3</sub> Solution by the Expired Tylosin Drug. *Biointerface research in applied chemistry* **2022**, *12*, 5116–5130, <https://doi.org/10.33263/BRIAC124.51165130>.
44. Rani, A.T.; Thomas, A.; Williams, L.; Joseph, A. Effect of Lunamarine, the Major Constituent of *Boerhaavia diffusa* Leave Extract on the Corrosion Inhibition of Mild Steel in Hydrochloric Acid; Computational Modelling, Surface Screening and Electroanalytical Studies. *Journal of Bio-and Tribo-Corrosion.* **2022**, *8*, 1-21, <https://doi.org/10.1007/s40735-021-00616-2>.
45. Schweinsberg, D.P.; George, G.A.; Nanayakkara, A.K.; Steinert, D.A. The protective action of epoxy resins and curing agents—inhibitive effects on the aqueous acid corrosion of iron and steel. *Corros Sci.* **1988**, *28*, 33-42, [https://doi.org/10.1016/0010-938X\(88\)90004-2](https://doi.org/10.1016/0010-938X(88)90004-2).